Dipolar 1,3-cycloaddition of thioformaldehyde *S*-methylide (CH$_2$SCH$_2$) to ethylene and acetylene. A comparison with (valence) isoelectronic O$_3$, SO$_2$, CH$_2$OO and CH$_2$SO.

Zoi Salta[1*], Mauricio Vega-Teijido[2], Aline Katz[2], Nicola Tasinato[1], Vincenzo Barone[1], and Oscar N. Ventura[2]

[1]*Scuola Normale Superiore, piazza dei Cavalieri 7, 56126 Pisa, Italy*

[2]*Computational Chemistry and Biology Group, CCBG, DETEMA, Facultad de Química, Universidad de la República, 11400 Montevideo, Uruguay*

ABSTRACT: Methods rooted in the Density Functional Theory and in the coupled cluster ansatz were employed to investigate the cycloaddition reactions to ethylene and acetylene of 1,3-dipolar species including ozone and the derivatives issued from replacement of the central oxygen atom by the valence-isoelectronic sulfur atom, and/or of one or both terminal oxygen atoms by the isoelectronic CH$_2$ group. This gives rise to five different 1,3-dipolar compounds, namely ozone itself (O$_3$), sulfur dioxide (SO$_2$), the simplest Criegee intermediate (CH$_2$OO), sulfine (CH$_2$SO) and thioformaldehyde *S*-methylide (CH$_2$SCH$_2$, TSM). The experimental and accurate theoretical data available for some of those molecules were employed to assess the accuracy of two last-generation composite methods employing conventional or explicitly correlated post-Hartree-Fock contributions (jun-Cheap and SVECV-f12, respectively), which were then applied to investigate the reactivity of TSM. The energy barriers provided by both composite methods are very close (the average values for the two composite methods are 7.1 and 8.3 kcal·mol^{-1} for the addition to ethylene and acetylene, respectively) and comparable to those ruling the corresponding additions of ozone (4.0 and 7.7 kcal·mol^{-1}, respectively). These and other evidences strongly suggest that, at least in the case of cycloadditions, the reactivity of TSM is similar to that of O$_3$ and very different from that of SO$_2$.

Key words: 1,3-cycloaddition, thiocarbonyl ylides, density functional theory, coupled cluster methods, cost-effective composite methods.

*Corresponding author: Dr. Zoi Salta, SMART Lab, Scuola Normale Superiore Piazza dei Cavalieri

56126 Pisa, Italy, E-mail: Zoi.Salta@sns.it

ORCID:

Zoi Salta (0000-0002-7826-0182),

Mauricio Vega-Teijido (0000-0002-7120-7979),

Aline Katz (0000-0001-5134-8400),

Nicola Tasinato (0000-0003-1755-7238),

Vincenzo Barone (0000-0001-6420-4107),

Oscar N. Ventura (0000-0001-5474-0061)

1. INTRODUCTION

Heterocyclic compounds represent one of the most complex and intriguing families of organic molecules, whose interest spans from remarkable theoretical implications to challenging synthetic procedures, not to mention physiological and industrial significance. Cycloaddition reactions play a key role in both synthetic and mechanistic organic chemistry and the current understanding of the underlying principles in this area has strongly benefited from an effective synergism between theory and experiment. The pioneering work of Huisgen and co-workers[1] introduced the general concept of 1,3-dipolar cycloaddition, which represented in recent years a crucial step in the synthetic routes toward a number of natural and synthetic products.[2]

1,3-dipolar cycloadditions are generally described as pericyclic processes,[3–6] involving the formation of two new σ bonds, with a concerted mechanism being allowed by orbital symmetry rules for $[\pi_{4s} + \pi_{2s}]$ cycloadditions. The mechanistic picture is influenced not only by the nature of the substituents, but also by the kind and number of heteroatoms in the 1,3-dipole. Those species can react in either stepwise or concerted ways, and Huisgen was the first to establish a rationale for the concerted mechanism.[3–5] On the other hand, Firestone proposed a stepwise mechanism involving diradical intermediates.[7] In that mechanism, an unstable diradical intermediate cyclizes, maintaining stereospecificity before the C-C bond rotates. These studies, mostly based on the stereospecific outcome, led to a consensus about the preference for a concerted process with respect to the stepwise mechanism.[8–10]

Thiocarbonyl ylides belong to the family of sulfur-centered 1,3-dipoles characterized by the presence of two sp^2 C atoms attached to the sulfur atom. In comparison with other 1,3-dipoles that have been extensively explored in organic synthesis, these ones [11–15] are still quite poorly characterized. However, within the last decades, remarkable progress has been made regarding

both methods of generation and synthetic applications, so that thiocarbonyl ylides are becoming key intermediates in the synthesis of sulfur-containing heterocyclic compounds.

Systematic studies of the nitrogen elimination from 2,5-dihydro-1,3,4-thiadiazoles by Kellogg and co-workers[16,17] were the first to demonstrate that thiocarbonyl ylides are reactive intermediates that can undergo either an electrocyclization reaction to give thiiranes or to be trapped by suitable dipolarophiles to produce sulfur-containing five-membered heterocycles. Like other 1,3-dipolar species, thiocarbonyl ylides are able to participate in intra- and inter-molecular cycloaddition reactions. Because of that, they seem to have a great potential for the synthesis of many sulfur-containing systems in a stereo-controlled manner.

The parent compound of the thiocarbonyl ylide family, thioformaldehyde *S*-methylide (TSM), was initially recognized by Knott in 1955[18] and later studied by several research groups using different spectroscopic and theoretical methods.[11–15,19,20] However, after the work by Sustmann et al. in 2003[20] concerning the mechanism of cycloaddition of thioformaldehyde *S*-methylide, the only available theoretical studies are those performed in the last two years by our groups.[21–23] In particular, we started by proposing an original path leading to TSM based on a detailed computational study of the H-abstraction path in the oxidation of dimethyl sulfide (DMS) by OH radicals, under the hypothesis of high OH concentration.[21,22] We identified a reaction channel that could be open for the transformation of DMS into a closed shell planar structure where two methylene groups are bound to the central sulfur, namely TSM. Next, we discussed the structural details in the context of the stationary points ruling the [SC$_2$H$_4$] potential energy surface (PES).[23] Further studies on the reactivity of TSM are of current interest, and in this paper we analyze in detail its behavior in 1,3-dipolar cycloadditions, with specific reference to the well-known process of ozonolysis.

Ozonolysis represents one of the most important oxidation reactions of species with unsaturated bonds,[24–26] which are key processes for both organic synthesis[27] and materials chemistry.[28] Nearly all the proposed mechanisms for this reaction involve the initial rate determining 1,3-dipolar cycloaddition of ozone to the double or triple bond, forming primary ozonides.[29] The description of reactions involving ozone is complicated by its diradical character, which has been estimated around 33% by natural orbital occupation and generalized valence bond computations.[30–32] In the computational study performed by Wheeler et al.,[33] the barriers for the concerted cycloaddition of ozone with acetylene and ethylene were determined through the systematic extrapolation of post-Hartree-Fock energies within the so called focal point approach. The results of a more recent study by Saito et al.[34] devoted to the concerted and stepwise mechanism for ozonolysis of ethylene and acrylonitrile confirmed the preference for a concerted path in both cases.

In parallel, it has been shown that even though ozone and sulfur dioxide are valence isoelectronic, they show a very different reactivity. While O_3 is one of the most reactive 1,3-dipoles, SO_2, in which the central oxygen atom of O_3 is replaced by sulfur, is much less reactive. [35] A study by Lan et al.[36] suggested that the prohibitive barriers in the case of SO_2 arise from large distortion energies as well as unfavorable interaction energies in the transition states, related to the significant increase of the HOMO-LUMO gap when going from O_3 to SO_2. Furthermore, valence bond calculations showed that the significant diradical character of O_3 is practically absent in SO_2, whose main resonance structures involve either double bonds between sulfur and both terminal oxygens (with a sulfur octet expansion) or single bonds between a doubly positively charged central S atom and singly negatively charged end oxygen atoms (a so-called dritterion). Takeshita et al.[37] used generalized valence bond (GVB) theory[38] to characterize the electronic structure of

ozone and sulfur dioxide, showing that O_3 does indeed possess significant diradical character, whereas SO_2 is effectively a closed shell molecule. Finally, Braïda et al.[39] studied O_3 and its sulfur-substituted isomers by means of the Breathing Orbital Valence Bond *ab initio* method, with the objective of estimating their controversial diradical characters. They concluded that ozone has a large diradical character, between 44 and 49%, while SO_2 can be safely described as a closed-shell zwitterion.

Carbonyl oxides, also known as Criegee intermediates (CI), are key intermediates in the ozonolysis of unsaturated compounds, coming from the fragmentation of primary ozonides. The theoretical works performed till 2012 were reviewed by Vereecken and Francisco.[40] Since then, several interesting theoretical studies have been published, including work on the CI + O_3[41] and CI + carbonyl reactions.[42] Contrary to previous assumptions,[43] CIs are now known to be mostly zwitterionic[40,44,45] with a relatively low biradical character. The analogous zwitterionic structure with positively and negatively charged central and end atoms (1,3-dipoles) suggests a reactivity similar to that of ozone. In a more recent work, Vereecken et al.[46] characterized the reactions of CI with alkenes, CH_2OO, and O_3. They found that the reaction of CI with olefines is highly dependent on the presence and nature of substituents in the alkene and CI, with very large differences in the predicted rate coefficients. At the same time, Buras et al.[47] performed experimental rate measurements for the reaction of the simplest Criegee intermediate with C2−C4 alkenes by using laser flash photolysis, while the latest mechanistic study of the reaction of CIs with ethylene and acetylene was presented by Sun et al.[48]

The simplest CI, CH_2OO, can be obtained by formal replacement of one terminal oxygen atom in ozone by the isoelectronic CH_2 group. A similar formal substitution can be done in SO_2 and the resulting species is the simplest sulfine, CH_2SO. Sulfines are four-centered

heterocumulenes with general formula $R_1R_2C=S=O$. While sulfines with R_1 and R_2 different from H are generally stable compounds, sulfines with R_1 and/or R_2 = H are relatively unstable and do not survive for a long time at room temperature.[49] Many sulfines have been synthesized,[50] but it was not until 1976 that the parent molecule $CH_2=S=O$ was prepared in the gas-phase,[51] and characterized.[51–53] Formally, the structure of this molecule can be written either in a neutral or dipolar form and both resonance structures can be recognized in a valence bond decomposition of the electronic distribution. Although some theoretical studies are available concerning its thermochemical properties[54] (and references therein) and the dimerization reaction,[55] to the best of our knowledge its ability to participate in cycloaddition reactions has not been yet investigated.

Ozone

Sulfur dioxide

Thioformaldehyde *S*-methylide
(TSM)

Formaldehyde oxide
(Criegee intermediate)

Thioformladehyde *S*-oxide
(Sulfine)

Ozone

Sulfur dioxide

Formaldehyde S-methylide
(TSM)

Formaldehyde oxide
(Criegge intermediate)

Formaldehyde S-oxide
(Sulfine)
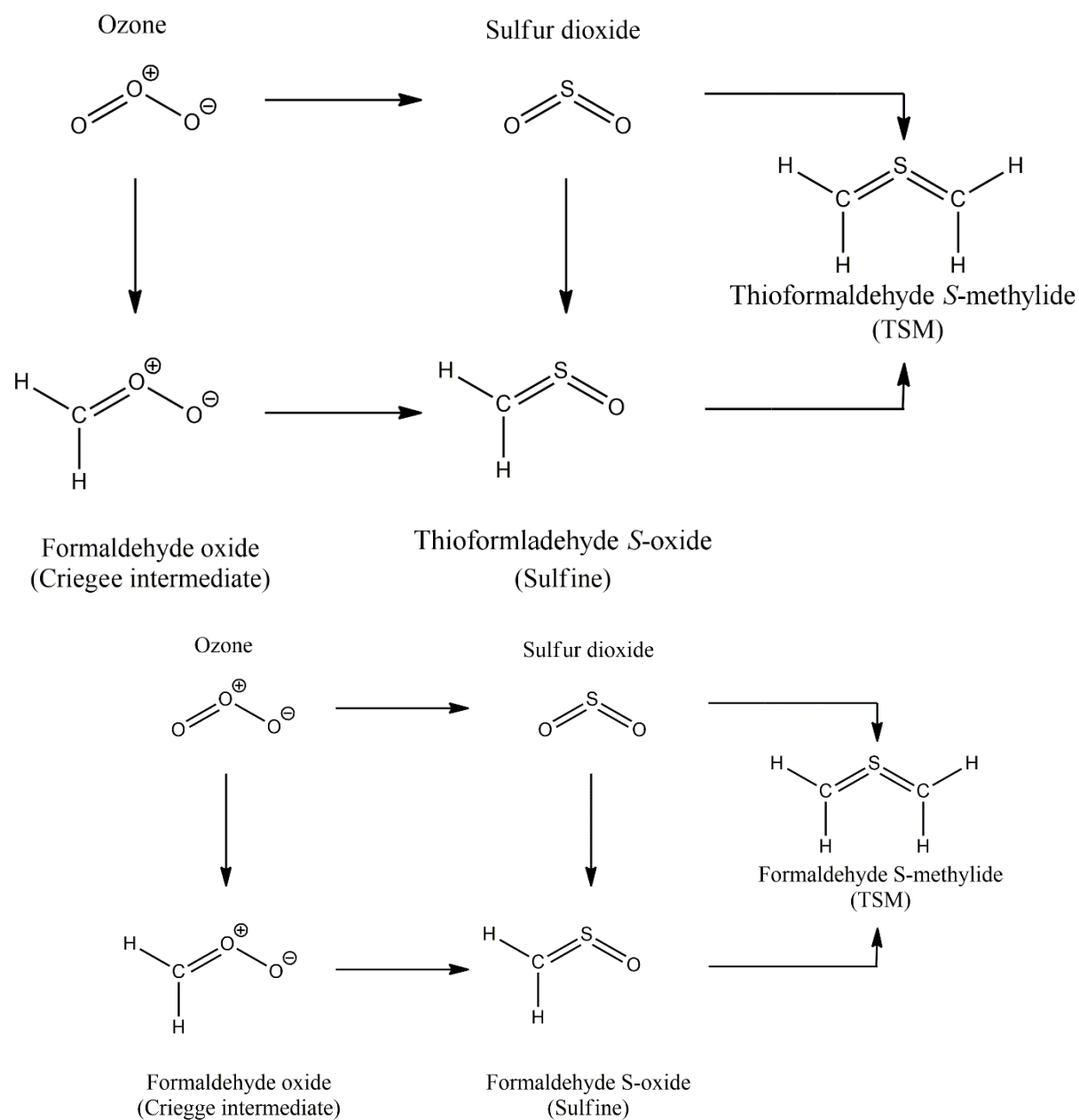
Scheme 1. Relationships and nomenclature of the five reactants employed in this work.

The main purpose of this paper is to report the most significant results of a comprehensive theoretical study on the 1,3-dipolar cycloaddition to ethylene and acetylene of the five stable isoelectronic (or valence isoelectronic) compounds presented in Scheme 1, which can be obtained from O_3 or SO_2 replacing one or both the terminal oxygen atoms by the isoelectronic CH_2 moiety.

In particular, the study aims to determine whether the reactivity of TSM toward ethylene and acetylene is closer to that of O_3 or SO_2 and to rationalize the results by means of different energy decomposition analyses.

2. COMPUTATIONAL METHODS

A number of models rooted in the density functional theory (DFT), as well as different post-Hartree-Fock composite schemes were employed to study the structure and energetics of all the considered species. Specifically, the ωB97X-D,[56] M06-2X,[57] and rev-DSDPBEP86[58] functionals were used, in conjunction with the jun-cc-pV(T+d)Z basis set.[59] The extension of the basis set with tight d functions is known to be important for a quantitative description of the electronic structure of third-row atoms (sulfur in our case).[60,61] In order to account for dispersion interactions, M06-2X and rev-DSDPBEP86 were augmented by Grimme's DFT-D3 semiempirical dispersion,[62,63] which has been applied with considerable success to a large number of different systems, including dimers, large supramolecular complexes and reaction energies/barriers. The well-documented CBS-QB3,[64] G4,[65] and W1BD[66] composite methods were used in their original implementations, together with the more recent SVECV-f12[67] and jun-ChS[68,69] models. SVECV-f12, in the implementation used in this paper, employs M06-2X-D3/jun-cc-pV(T+d)Z optimum geometries to perform CCSD(T)-F12b(3C/FIX)[70] complete basis set (CBS) single-point calculations (obtained by extrapolation of cc-pVDZ-F12 and cc-pVTZ-F12 results), augmented by core-valence correlation corrections at the MP2/cc-pCVTZ level. The jun-ChS approach employs rev-DSDPBEP86-D3(BJ)/jun-cc-pV(T+d)Z geometries and corrects CCSD(T)/jun-cc-pV(T+d)Z energies for the CBS error and core-correlation effects. These are evaluated by a two-point extrapolation[71] of MP2 energies using jun-cc-pV(T+d)Z and jun-cc-pV(Q+d)Z basis sets and as the difference between MP2/cc-pwCVTZ results obtained by correlating all and only valence

electrons, respectively. Some of the reactants were also studied using the CASSCF[72] and CASPT2[73] procedures, as described later in the text. In these cases, all the valence orbitals and electrons were included in the active space. Geometry optimizations were performed at the CASPT2 level, not the underlaying CASSCF one.

After performing geometry optimizations with very tight convergence criteria (e.g., 10^{-4} Å on Cartesian coordinates), Hessians were inspected to check the correct number of negative eigenvalues for all species. Analytical second derivatives were employed when available, whereas numerical derivatives of analytical gradients were used in the other cases. Intrinsic Reaction Coordinates (IRC)[74] were used to ensure that each saddle point connects the correct reactants and products.

A number of analysis tools were employed to study the bonding patterns in the transition states. The Natural Bond Orbital[75] (NBO) analysis was employed for determining the atomic charges. The analysis of the Lagrangian of the density according to Bader's theory of atoms in molecules (AIM) was performed to observe critical points on the electronic density distribution and bonding paths connecting atoms.[76] The root mean square difference between bond lengths in the transition states and the corresponding products was used as an index of the closeness of the TS to the final heterocyclic product. The HOMO-LUMO gap was also determined and used as a tool to explore the efficiency of charge transfer between the reactants and the unsaturated compounds.

All calculations were performed using the Gaussian 16[77] and Molpro 2020.1[78] programs. The AIM analysis was performed by employing the AIMPAC computer program.[79]

3. RESULTS AND DISCUSSION

3.1. Geometrical structure of the reactants. Figure 1 shows the structure of the reactants in the general processes

$$C_2H_4 + \text{dipolar reactant} \rightarrow \text{5-member saturated heterocycle} \qquad (1)$$

$$C_2H_2 + \text{dipolar reactant} \rightarrow \text{5-member unsaturated heterocycle} \qquad (2)$$
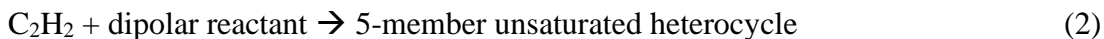
optimized at the M06-2X-D3 and rev-DSDPBEP86-D3(BJ) levels, using the jun-cc-pV(T+*d*)Z basis set, as well as at the CCSD(T)-F12b/cc-pVQZ-F12 level. In the case of O_3, CH_2OO, and CH_2SCH_2, which could involve non negligible multireference character, we employed also the CASPT2 method in conjunction with the aug-cc-pVQZ basis set, on top of a CASSCF(m,n) calculation. All the valence electrons and occupied orbitals were included in the MCSCF calculation for the three aforementioned species resulting in (m,n) = (18,12) for O_3, (18,14) for CI, and (16,16) for TSM. Geometry optimizations were performed at the CASPT2 level.

The bond lengths of the heavy atom skeleton collected in Fig. 1 are systematically underestimated at the M06-2X-D3 level (in average by 0.01 Å) with the OO and CO bonds in O_3 and CI showing the largest errors (0.047 Å and 0.030 Å, respectively). The only exception is represented by the OO bond length in CI, which is only 0.002 Å longer than the best semi-experimental estimate.

Concerning the rev-DSDPBEP86-D3(BJ) functional, a detailed analysis of its performance in predicting structural parameters, including C-S bond lengths, has already been carried out by Ceselin et al.[80] who have also proposed the Nano-LEGO tool to improve the accuracy of the bare functional. Briefly, the approach, that has been already successfully applied to a number of molecules [80, G. Ceselin et al. J. Phys. Chem A, 126, 2373-2387, 2022; A. Pietropolli Charmet et al, Molecules, 27, 748 (2022)], is based on a systematic assessment of the errors between DFT

equilibrium geometries and accurate semi-experimental equilibrium structures. Then, a combination of two methods, namely the linear regression approach (LRA) [Piccardo et al. J. Phys. Chem. A, 119, 2058-2082, 2015] and the template molecule (TMA) [Penocchio et al. JCTC, 4689-4707 (2015), Penocchio et al. Can. J. Chem. 1065-1076 (2016)] is employed for correcting the computed bond lengths and angles. The former stems from the use of linear regressions to rectify the systematic errors affecting DFT equilibrium geometries; on the other hand, the TMA can be thought as a generalization, in which the correction term is evaluated based on a similar molecule, acting as a template, for which an accurate semi-experimental equilibrium geometry is available. Here, we point out that the error on the bond lengths of the heavy atom skeleton is well below 0.01 Å in absolute value, with the only exceptions (0.011 and -0.017 Å) being represented by the SO and OO bond lengths of SO_2 and CI, respectively. Since the semi-experimental structure of TSM is not available, application of the nano-LEGO correction to the rev-DSDPBEP86-D3(BJ) result (1.630) leads to an estimate of 1.627 Å with an error bar of 0.001 Å. Also in this case, the M06-2X-D3 functional underestimates the bond length by more than 0.01 Å.

a) 1.322
b) 1.332
d) 1.330
e) 1.331

a) 1.194
b) 1.206
d) 1.201
e) 1.203
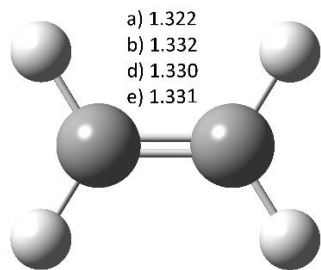
Ethylene (ETH)   Acetylene (ACE)

a) 1.231
b) 1.274
c) 1.266
d) 1.280
e) 1.278

a) 1.425
b) 1.442
d) 1.429
e) 1.431

a) 1.239
b) 1.270
c) 1.269
d) 1.279
e) 1.270

a) 1.342
b) 1.324
c) 1.341
d) 1.335
e) 1.341

Ozone (O_3)   Sulfur Dioxide (SO_2)   Criegee Intermediate (CI)

a) 1.595
b) 1.612
d) 1.606
e) 1.608

a) 1.463
b) 1.473
d) 1.465
e) 1.465

a) 1.614
b) 1.630
c) 1.642
d) 1.627.

Thioformaldehyde *S*-oxide
(FSO)

Thioformaldehyde *S*-methylide (TSM)
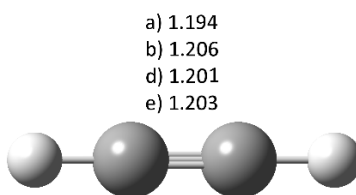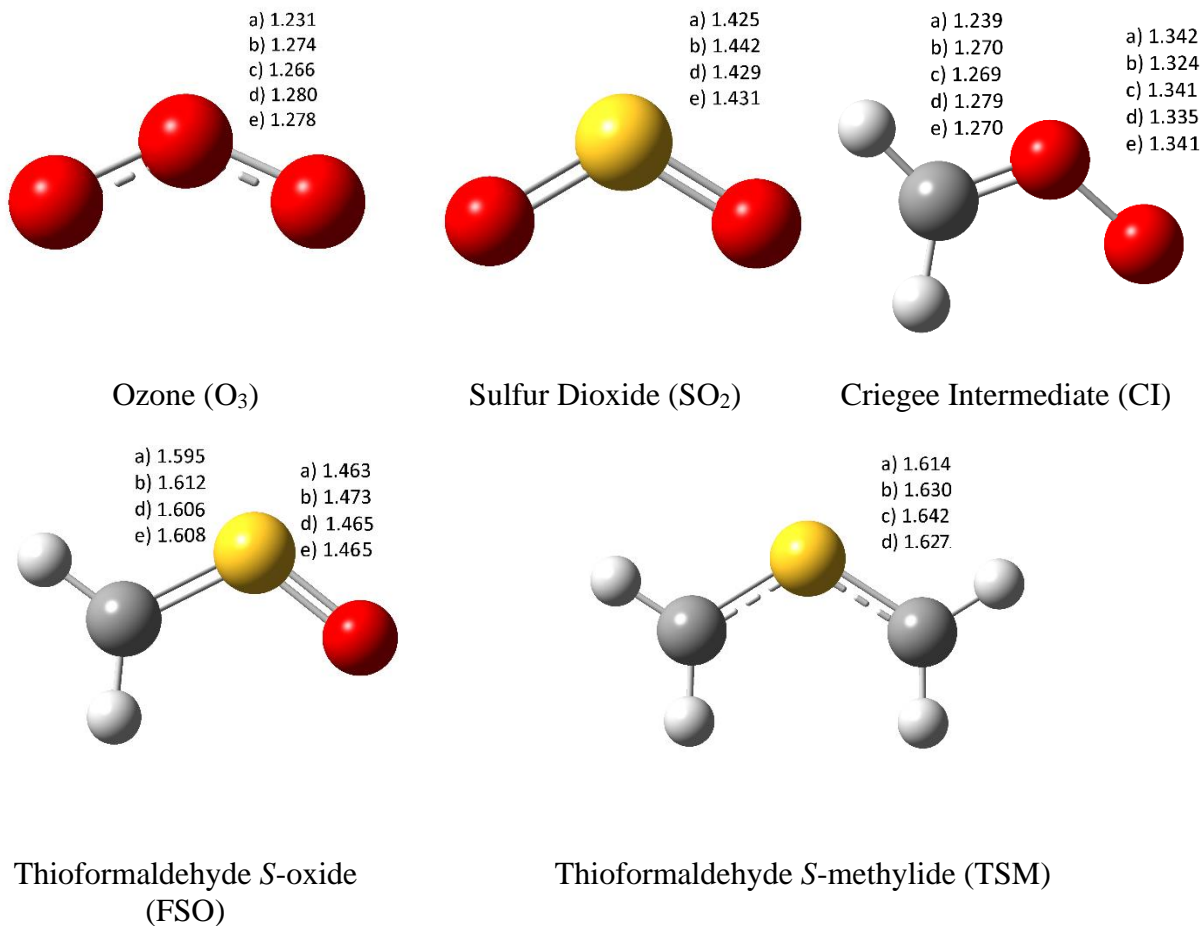
Figure 1. Bond lengths (in Å) of the heavy-atom backbone of the reactants studied in this paper. Labels for the parameters are as follows: a) M06-2X-D3/jun-cc-pV(T+*d*)Z, b) rev-DSDPBEP86-D3(BJ)/jun-cc-pV(T+*d*)Z, c) CASPT2/CASSCF(m,n) (m,n = 18,12 for O_3, 18,14 for CI, and 16,16 for TSM), d) CCSD(T)-F12/cc-pVQZ-F12 and e) experimental (ETH, references[80,81]; ACE, references[80,82]; O_3, reference[81]; SO_2, references[61,81]; CI, references[45,83]; FSO, reference[84]).

Interestingly, the CO bond length predicted for the Criegee intermediate by the rev-DSDPBEP86-D3(BJ) functional is very accurate, whereas M06-2X-D3 performs a better job for the corresponding OO distance. All in all, both the tested functionals provide fairly accurate results for the reactants considered in this work, with the double-hybrid rev-DSDPBEP86-D3 functional leading to slightly lower errors.

As mentioned above, another interesting aspect to consider concerns the diradical character of O_3, CI and TSM. Qualitative considerations can be based on a comparison between single

reference (CCSD(T)) and multireference (CASPT2) computations, but a fully quantitative analysis is not possible since dynamical correlation is better described by the former approach and non-dynamical correlation by the second one. In the same vein, although spin contamination of unrestricted approaches is a diagnostic of diradical character, it has not the same meaning in Kohn-Sham and Hartree-Fock models, mainly because the KS orbitals do include already correlation energy when optimized, while the HF ones do not. Additional information can be drawn from the T1[85–88] and D1[89–91] diagnostics in CCSD(T)-F12/cc-pVTZ-F12 calculations. There is a general agreement that a single-configuration wave function can be used when T1 < 0.02[85,86] and D1 < 0.05[92], although larger values have been proposed in some cases[93]. These values are collected in Table 1 together with the ratio T1/D1 which, according to Lee,[91] is a measure of the electronic structure homogeneity (the larger the deviation from 1/2, the more inhomogeneous the system). Inspection of this table suggests that TSM and SO_2 are the least inhomogeneous systems, thus being the species better described overall at the CCSD(T) and CCSD(T)-F12 levels. Since the molecules are small enough, both D1, which is size consistent, and T1, which is not, give the same information, with TSM showing the smallest T1 diagnostic, i.e. being again the species best described by the single reference CCSD(T)-F12/cc-pVTZ-F12 model.

Actually, if one accepts the limits mentioned above for T1 and D1, only TSM should be safely amenable to single-reference computations and CI can be described only by multi-reference approaches. However, as already mentioned in previous studies,[44,45] both the dominant electronic configurations of CI are closed-shell, meaning that this species is not a biradical and could be reasonably described by a highly correlated single reference method.

Table 1. Diagnostics of multi-configurational character of the CCSD(T)-F12/cc-pVTZ-F12 calculations.

Species	T1 Diagnostic	D1 diagnostic	Ratio T1/D1
O_3	0.024	0.066	0.364

CI	0.040	0.160	0.250
TSM	0.016	0.041	0.390
SO$_2$	0.023	0.058	0.397
FSO	0.020	0.064	0.313

A further indication of the multireference character of a molecular system is provided by the square of C_0, the coefficient of the dominant configuration in the CASSCF treatment, with a value of 0.90 or larger being generally considered sufficient for a single reference treatment. The values we obtained (0.63 for CI, 0.83 for O$_3$ and 0.89 for TSM) are consistent with the other estimates in indicating that TSM fulfills this requirement, whereas more attention should be paid to O$_3$ and, especially, CI. However, previous computations and the other considerations given above suggest that CCSD(T)-F12 computations in conjunction with extended basis sets could provide reasonable results for all the considered species.

3.2. NBO charges and HOMO-LUMO gap of the reactants. Other interesting semi-quantitative considerations can be based on the NBO charge distributions of the reactants computed by the M06-2X and rev-DSDPBEP86 functionals and shown in Figure 2.

O₃ · SO₂ · CI

FSO · TSM
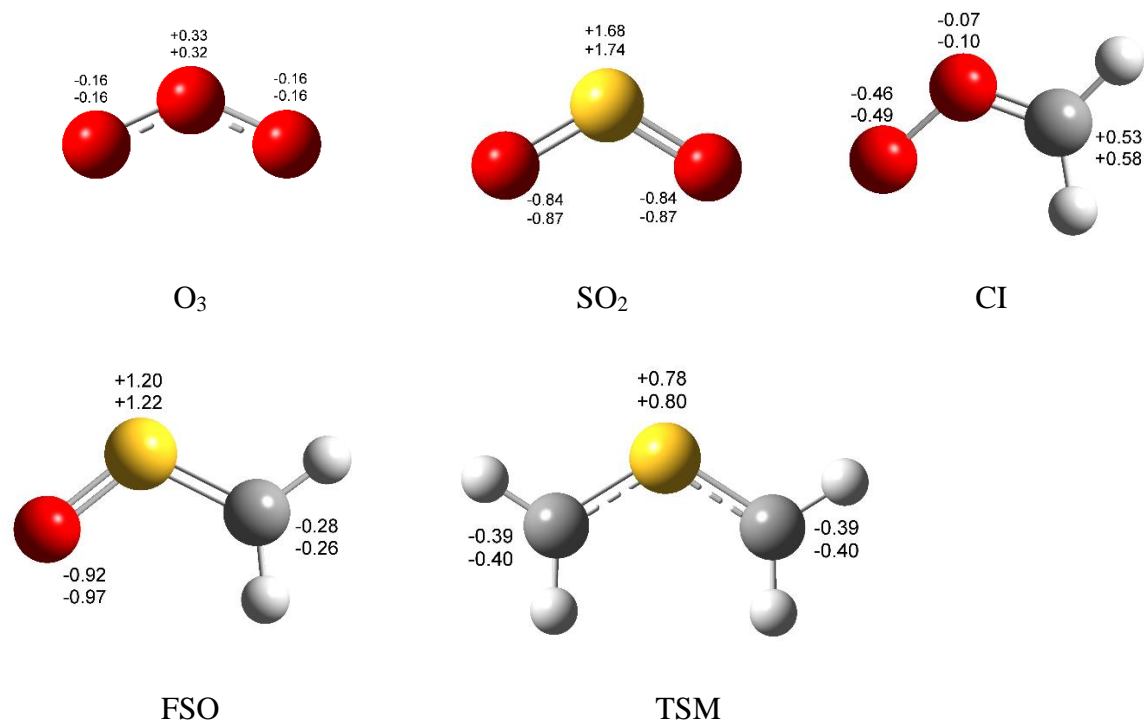
Figure 2. NBO charges for the dipolar reactants at the M06-2X-D3 (upper entry) and rev-DSDPBEP86-D3(BJ) (lower entry) levels of theory. Carbon and hydrogen charges are added up and the CH_2 charge is reported.

The contribution of intermolecular charge transfer to the interaction between the dipolar species and the olefin (ETH, ACE) can be assessed in at least two ways. First, one can analyze the HOMO-LUMO gap in the five dipolar molecules and the energy difference between the HOMO of ETH and ACE and the LUMO of the dipolar molecules, since charge transfer occurs from HOMO(X) to LUMO(Y) where X = ETH or ACE and Y = O₃, SO₂, CI, FSO or TSM. These values are collected in Table 2. Second, one can analyze the differences of the NBO charges of the different atoms in the TSs and in the reactants.

Concerning the first analysis, it is apparent that the HOMO and LUMO of the dipolarophiles are very similar, so that any difference in the reactivity should be ascribed to the 1,3-dipolar species. However, it should be mentioned that this trend does not correlate well with

that observed employing Hartree-Fock molecular orbitals.[6] Kohn-Sham orbitals are projections of the electronic density into a mono-determinant function, so that they reflect all the correlation energy included in the potential used to calculate the electronic density. On the contrary, Hartree-Fock orbitals do not include correlation, except, possibly, spin-polarization if a UHF procedure is employed. One of the consequences is that Koopmans theorem does not apply directly to KS orbitals.

Table 2. Energy (eV) of the HOMO/LUMO of the reactants, their energy difference, and difference between the HOMO of the dipolar reactants and the LUMO of ETH and ACE.

	E_{HOMO}		E_{LUMO}		$\Delta (E_{HOMO} - E_{LUMO})$		$\Delta 1(E_{HOMO} - E_{LUMO})^a$		$\Delta 2(E_{HOMO} - E_{LUMO})^b$	
Species	M062X	revDSD	M062X	revDSD	M062X	revDSD	M062X	revDSD	M062X	revDSD
ETH	-9.2	-9.4	0.6	1.2	-9.8	-10.6				
ACE	-9.8	-10.1	0.5	1.1	-10.3	-11.2				
O_3	-11.7	-12.2	-3.7	-3.1	-8.1	-9.1	12.3	13.4	12.2	13.3
SO_2	-11.2	-12.0	-2.4	-1.5	-8.8	-10.5	11.8	13.2	11.7	13.1
CI	-8.8	-9.2	-1.7	-0.7	-7.1	-8.5	9.4	10.4	9.3	10.3
FSO	-9.1	-9.4	-1.3	-0.4	-7.8	-9.1	9.7	10.7	9.6	10.6
TSM	-6.8	-6.9	-0.6	0.3	-6.2	-7.2	7.8	8.1	7.3	8.0

$^a\Delta 1(E_{HOMO} - E_{LUMO}) = E_{HOMO(reactant)} - E_{LUMO(ethylene)}$; $^b\Delta 2(E_{HOMO} - E_{LUMO}) = E_{HOMO(reactants)} - E_{LUMO(acetylene)}$

Although the choice of the functional has a non-negligible effect on the HOMO-LUMO gap between the 1,3-dipolar species and the dipolarophiles, with differences even larger than 1 eV, the trend of the differences is approximately the same, with TSM showing the smallest gap (lowest LUMO energy), followed by CI and FSO. We will see later that the order of reactivity in terms of the barriers is CI > O_3 > TSM > FSO > SO_2, so that the HOMO-LUMO gaps with respect to ETH or ACE cannot be considered the driving forces for the reaction.

The HOMO-LUMO separation within the dipolar species correlates better with the aforementioned order, but not completely. For a given dipolarophile, any difference in the reactivity must be ascribed to the geometric and/or electronic structure of the 1,3-dipolar species. It was shown and explained earlier why the substitution of the central oxygen atom in O_3 by a

sulfur atom to give SO_2 reduces dramatically the reactivity, but this result is not mirrored by the HOMO-LUMO gaps shown in Table 2. On the other side, substituting a terminal oxygen either in O_3 or SO_2 by the isoelectronic CH_2 group (leading to CI or FSO), lowers the energy gap, but also adds some steric constraint, since both species should go from the planar configuration in the isolated molecule to a non-planar one in the transition state.[4] The same is true for the substitution of the second oxygen in FSO by a methylene group, which again lowers the gap and should add some additional deformation energy. Actually, according to Breugst et al.,[6] (a review of the original paper of Lan, Wheeler and Houk[36]) the activation barriers correlate much better with the distortion energies than with the interaction energies. In conclusion, frontier orbital analysis appears unable to fully explain the reactivity of these species, but it remains to be seen whether geometry distortion does play or not a major role.

3.3. Geometrical and electronic structure of products and transition states. The products of the reactions of the five dipolar species with ETH and ACE are shown in Figure 3. All these heterocycles are stable, but only the products of the reaction of TSM with either ETH or ACE do not have any covalent bond between heteroatoms. All these species are too large for full CCSD(T)-F12/VQZ-F12 calculations with our present resources. Therefore, only DFT results are shown. The optimized geometries will be used later for the composite procedures mentioned in the computational methods section.

We will focus our analysis on the two derivatives of thiophene, tetrahydrothiophene (**A5)** and 2,5-dihydrothiophene (**B5),** which structural parameters have been estimated on the grounds of microwave spectra.[94,95] According to both theory and experiment, **A5** is a puckered ring with three CC and two CS nearly identical bond lengths, whose theoretical values (1.525, 1.828 and 1.527, 1.833 Å at the M06-2X-D3 and rev-DSDPBEP86-D3(BJ) level, respectively) agree very
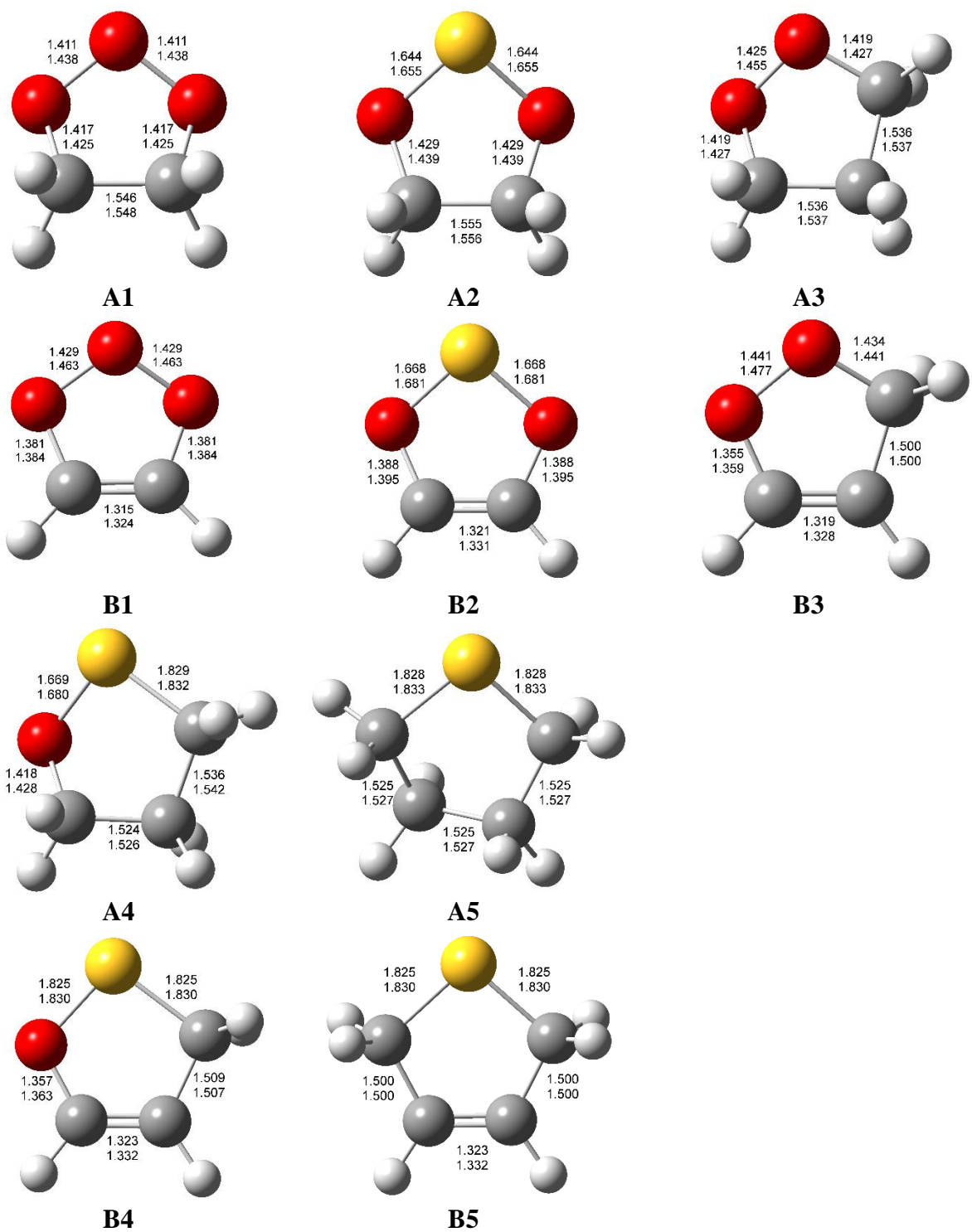
Figure 3. Bond distances in the ring structure of the products for the reactions of the five polar reactant, ETH and ACE. Results are shown at the M06-2X-D3 (upper entry) and rev-DSDPBEP86-D3(BJ) (lower entry) levels, using the jun-cc-pV(T+*d*)Z basis set. Bond lengths in Å.

well with the experimental counterparts (1.528 and 1.533Å for proximal and distal CC, respectively; 1.838 Å for CS).

The only previous theoretical studies of **A5** were performed about twenty years ago by El-Gogary[96] at the MP2/6-31G(d,p) level and more recently by Boese and Boese.[97] These latter authors named their optimized geometries as MP2/aug'-cc-pV[T,Q]Z + ΔQCISD(T)/aug-cc-pVDZ, which might be considered an approximation to CCSD(T)/CBS geometrical structures. The parameters obtained were 1.818, 1.537 and 1.554 Å for the CS, proximal CC and distal CC bonds respectively, but, unfortunately, they considered only the envelope form, which is not the absolute energy minimum. This could explain the much larger difference between distal and proximal CC bond lengths with respect to our computations and experiment.

In the case of **B5**, the theoretical CC bond lengths (1.323 and 1.332 Å for the single bonds or 1.500 and 1.500 Å for the double bond at the M06-2X-D3 and rev-DSDPBEP86-D3(BJ) level, respectively) are shorter than the experimental estimates (1.340 and 1.518 Å for the double and the single CC bond, respectively), whereas the opposite is true for the CS bond length (1.825, 1.830 and 1.816 Å from M06-2X-D3, rev-DSDPBEP86-D3(BJ) and experiment, respectively). Recently, Grant Hill and Legon optimized the structure of **B5** at the CCSD(T)-F12/VTZ-F12 level,[98] obtaining values close to our DFT ones (1.332, 1.500 and 1,826 Å for the C=C, C–C and C–S bond length, respectively). These results give further support to the use of the DFT structures of the products in the evaluation of the reactant- or product-like nature of the transition states ruling the addition of the different 1,3-dipoles to ethylene and acetylene.

The transition states corresponding to the addition to ETH and ACE are shown in Figure 4. Only the TSs of concerted mechanisms were investigated, since this is known to be the preferred mechanism for O_3 and CI. However, the rev-DSDPBEP86-D3(BJ) result for SO_2 was giving an

unexpected asymmetrical transition state TS2B that will be discussed later. Using the optimized structures of the TSs, we calculated the root mean square distance (RMSD) of the coordinates in the ring between the TSs and the products, obtaining the values collected in Table 3 (TS2B is not included because of the non-concerted character that is apparently given by the rev-DSDPBEP86-D3(BJ) method).

Table 3. Root mean square distance between the bond lengths in the ring at the TS and product geometries in Å.

ETH			ACE		
Species	M06-2X	rev-DSDPBEP86	Species	M06-2X	rev-DSDPBEP86
A1	0.17	0.15	B1	0.14	0.13
A2	0.14	0.12	B2	0.12	See text
A3	0.15	0.15	B3	0.13	0.14
A4	0.16	0.15	B4	0.15	0.15
A5	0.18	0.17	B5	0.15	0.14

It is clear from these results that the TS in the reaction path of TSM + ETH (**A5**) to give the hydrogenated thiophenes is the "earliest" one, i.e. the least product like. In the case of the reaction with ACE, the TS with FSO is the least product-like, while TSM comes inmediately after. This is probably due to the larger structural rearrangemet taking place with the rotation of the CH_2 moiety (see reference[6]). This deformation energy would play against the favorable factor of the large HOMO energy of TSM, as shown before, and as discussed by Domingo et al. for thiocarbonyl ylides.[99] These combined effects should affect also the height of the barriers.
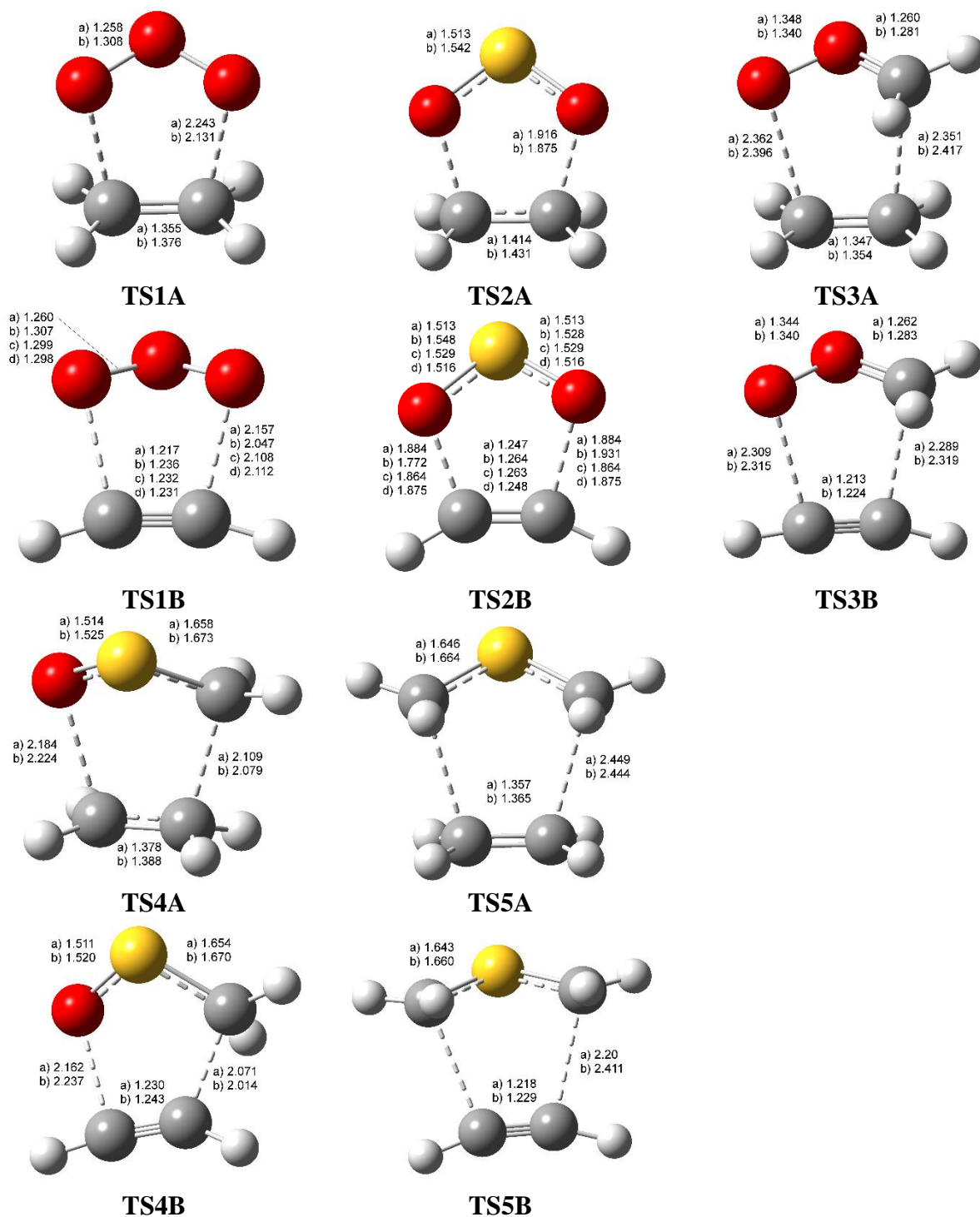
Figure 4. Structure of the transition states for the reactions of the five polar reactants with ETH and ACE. Results are shown at the a) M06-2X-D3 (upper entry) and b) rev-DSDPBEP86-D3(BJ) (lower entry) levels, using the jun-cc-pV(T+*d*)Z basis set. For TS1B and TS2B also optimized values at the c) CCSD(T)-F12/cc-pVDZ-F12 and d) CCSD(T)-F12/cc-pVTZ-F12 are included. Bond lengths in Å.

Examination ot the geometrical structure of the TSs shows that the two sets of DFT values present are consistent with each other even though there are some qualitative differences. For the symmetrical TSs ruling concerted paths (TS1A, TS2A, and TS1B), both the incoming bonds are longer at the rev-DSDPBEP86-D3(BJ) level, and in the case of TS2B (the addition of SO_2), M06-2X-D3 predicts a symmetric TS, whereas it is asymmetric at the rev-DSDPBEP86-D3(BJ)/jun-cc-pV(T+d)Z level of theory. In the case of the non-symmetric TSs (TS3A, TS4A, TS3B and TS4B), The more interesting cases are those of TS4A and TS4B, for which the forming CC bond is longer with M06-2X-D3 than with rev-DSDPBEP86-D3(BJ), but the opposite is true for the OC forming bond. As it can be seen in Fig. 3, this difference is not present in the final products.

To ascertain the quality of the DFT calculations, geometry optimizations were performed at the CCSD(T)-F12 level with the cc-pVDZ-F12 and cc-pVTZ-F12 basis sets for TS1B and TS2B. Looking specifically to TS1B, the CCSD(T)-F12 results obtained with the two different basis sets are quite close to each other, but the agreement with one or the other DFT model depends on the geometrical parameter considered. For the CO forming bonds, the CCSD(T)-F12 calculations are nearer to the M06-2X-D3 ones, for the increasing OO distance they come close to the rev-DSDPBEP86-D3(BJ) values and for the CC triple bond all the values are similar. Concerning TS2B, the obatined geometry appears very sensible to the basis set employed, indeed optimization with the rev-DSDPBEP86-D3(BJ) functional in conjunction with the larger aug-cc-pVQZ basis restored the symmetry of the transition state in agreement with CCSD(T)-F12 predictions. Our F12 results should be more accurate than those obtained by Lan et al.[36] at the CCSD(T)/cc-pV(T+d)Z level, but the values are basically in agreement exhibiting only small variations.

3.4. Bonding patterns at the transition states and hints about reactivity. A qualitative analysis of the bonding situation in the transition states can be performed by looking at the representation

of the electronic density in the plane containing both C atoms of the olefin and the two atoms of the dipolar molecule forming bonds with them. Alternatively, Bader's theory of atoms in molecules (AIM)[76] can be employed to find the critical points of the density and the paths interconnecting them. The images of the electronic density and of the AIM analysis are depicted in Figures 5 and 6.

Bader's analysis rests on the critical points on the electronic density $\rho(\mathbf{r})$. Chemical bonds are characterized by bonding critical points (BCP), i.e., points where the density decreases in two directions and increases in one. When and if bonds are formed in all sides of a ring structure, a ring critical point (RCP) is normally found near the center of gravity of the ring. This critical point corresponds to the situation where $\rho(\mathbf{r})$ increases in two directions and decreases in only one (along the axis perpendicular to the plane of the ring). Both BCPs and RCPs are present in the ten transition states shown in Figs. 5 and 6, displaying also the value (in a.u.) of the density at each critical point. The most interesting results are obtained for the TSs ruling the addition to acetylene, which will be discussed first.
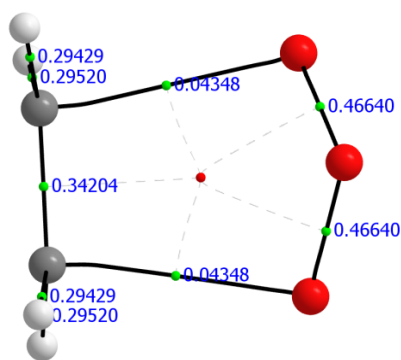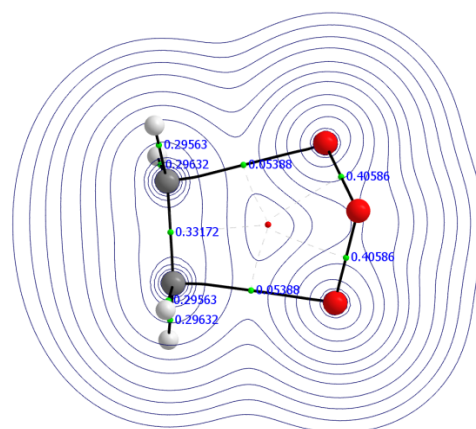
TS1A/M06   TS1A/DSD
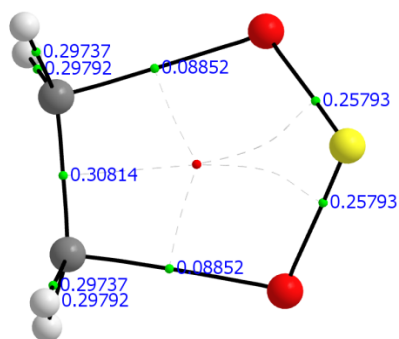
TS2A/M06
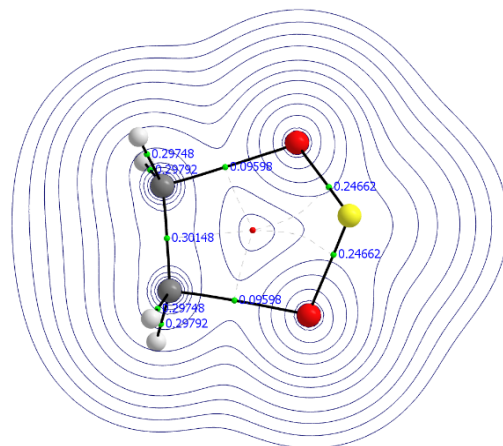
TS2A/DSD
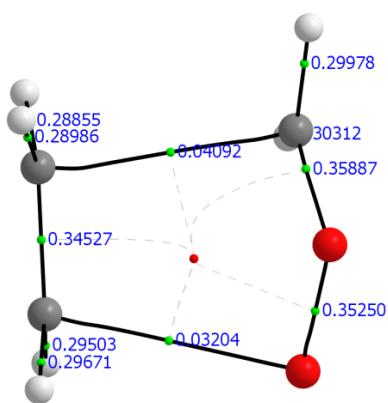
TS3A/M06
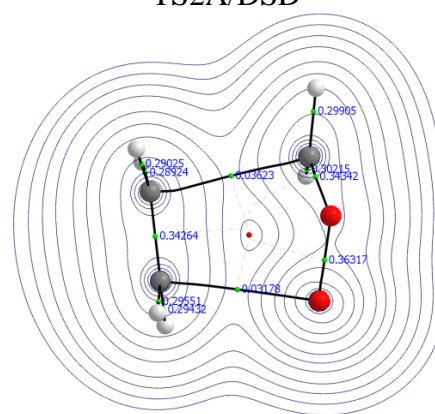
TS3A/DSD
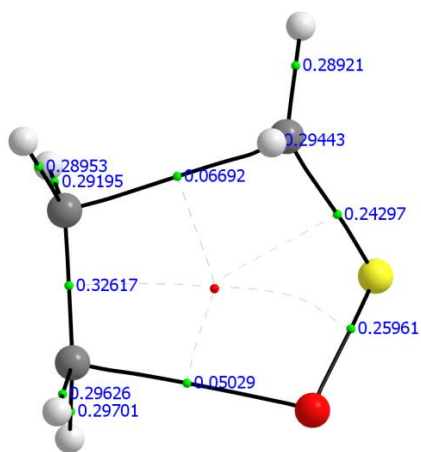
TS4A/M06
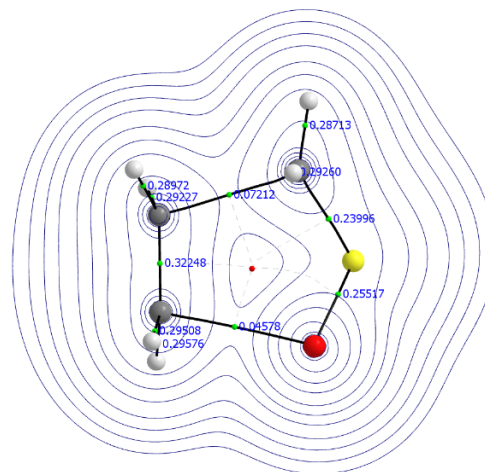
TS4A/DSD
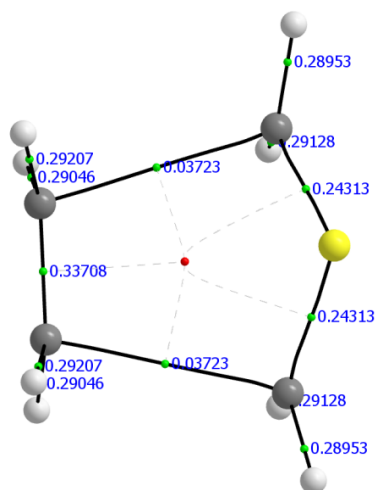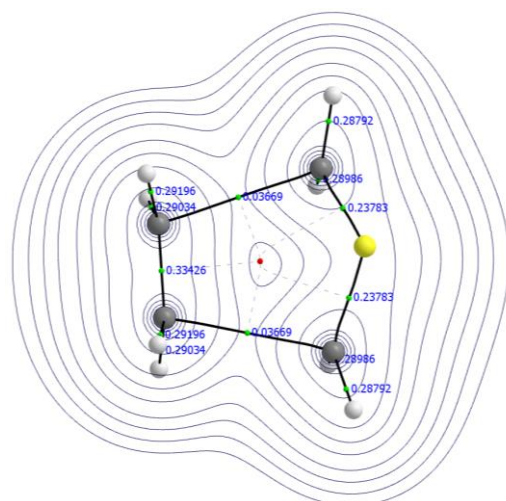
TS5A/M06   TS5A/DSD

Figure 5. Critical points of the electronic density and bonding paths interconnecting them according to AIM theory at the DFT theoretical levels used in this study for the ethylene dipolarophile. The isodensity values for the electronic density are shown only at the rev-DSDPBEP86-D3(BJ) level, in order to simplify the images.
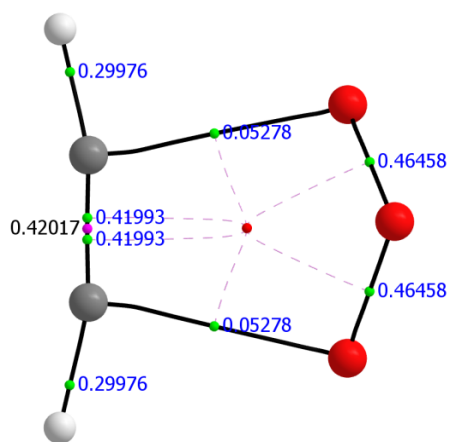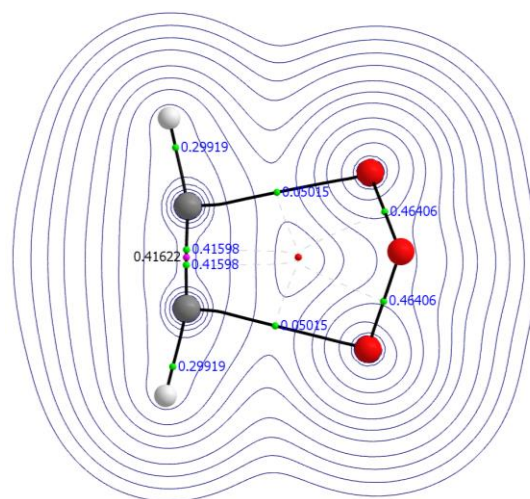
TS1B/M06   TS1B/DSD
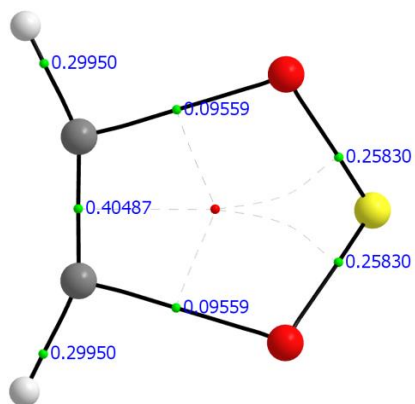
TS2B/M06
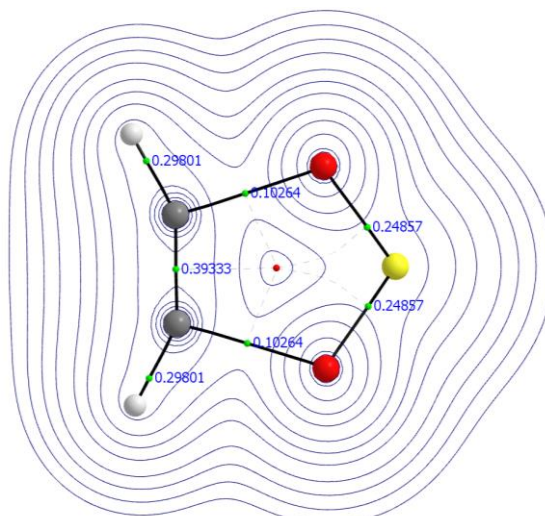
TS2B/DSD
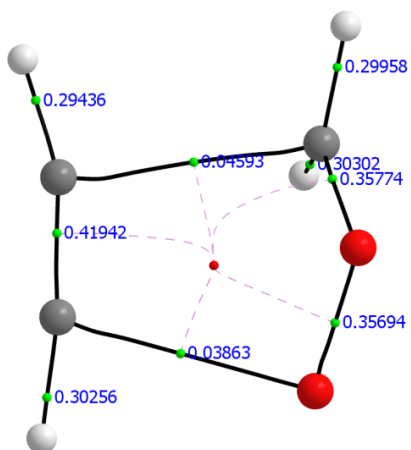
TS3B/M06
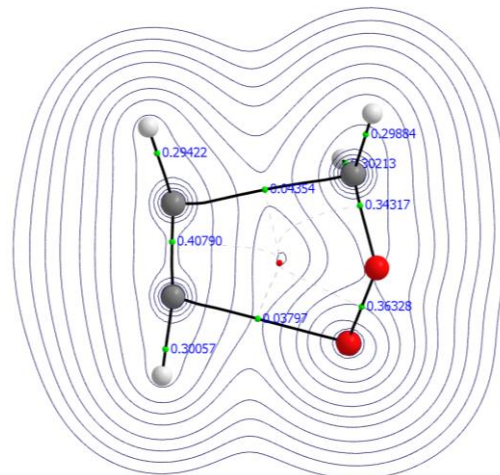
TS3B/DSD
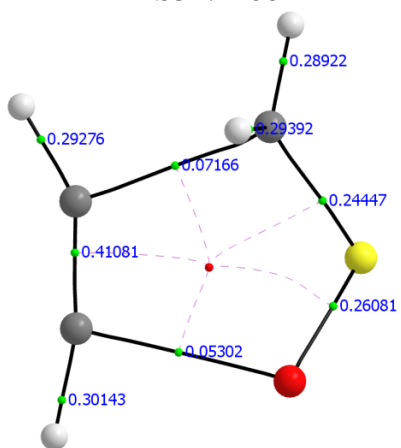
TS4B/M06
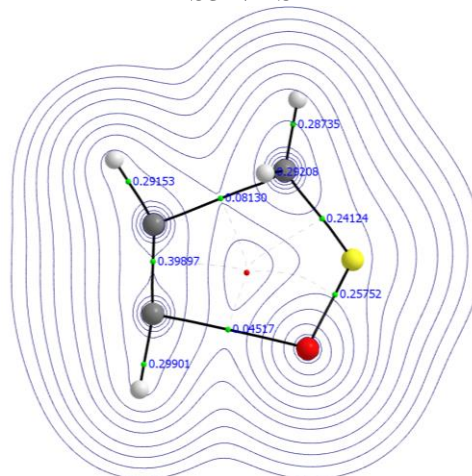
TS4B/DSD
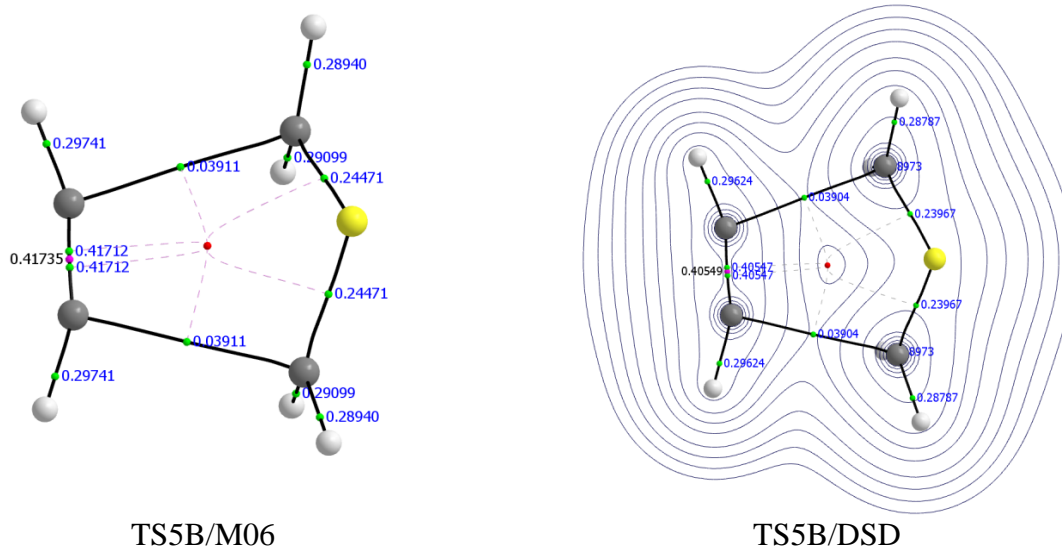
Figure 6. Critical points of the electronic density and bonding paths interconnecting them according to AIM theory at the DFT theoretical levels used in this study for the acetylene dipolarophile. The isodensity values for the electronic density are shown only at the rev-DSDPBEP86-D3(BJ) level, in order to simplify the images. The TS2B/DS image included here is the symmetry constrained one, see text below for a discussion.

Two different situations are observed: TS2B, TS3B and TS4B present only one BCP between the carbon atoms formerly in acetylene, while TS1B and TS5B present a more interesting arrangement. A critical point called a non-nuclear attractor (NNA), i.e., a critical point of the density which is a maximum in all directions, a (3,-3) CP in QTAIM theory, appeared in the middle of two identical BCPs. This slight electron density accumulation has been reported before in the literature for π bonds in acetylene complexes.[100,101] Other cases of NNA are well known in solids, and were experimentally observed, by X-ray diffraction, in Li-Na bonding or magnesium and beryllium crystals.[98,99] These observations of NNA have been supported by accurate calculations.

The similarity between TS1B and TS5B gives further support to the hypothesis that the reactivity of TSM is similar to that of O_3. The density at the BCP in TSM is smaller than in the case of O_3, with this supporting the view that TS5B is more reactant-like than TS1B, as observed also in the other analysis. The density values at the C-S BCP are similar to the ones observed in

the other TSs, but at the BCP of the forming C-C bonds, this TS5B exhibits the lowest values, again pointing towards a less advanced TS.

3.5. Energetic properties and trends in thermochemistry. The final stage of our analysis concerns reaction and activation energies. Table 4 collects the results obtained at different levels of theory: specifically, barriers and enthalpies of reaction have been evaluated by using rev-DSDPBEP86-D3(BJ) and M06-2X-D3 functionals coupled to the jun-cc-pV(T+d)Z basis set, as well as by using the ωB97X-D functional with the same basis set. In addition, a number of composite methods have been employed, including the jun-ChS and SVECV-f12 parameter-free composite methods and the CBS-QB3, G4 and W1BD models chemistries.

Reaction barriers obtained at different levels of calculation do not exhibit a large spread. Focusing on the reactions of O_3 and CI, the values are contained in the intervals [0.7 - 4.7] kcal·mol^{-1} and [-0.9 - 1.4] kcal·mol^{-1} for ETH, and [4.4 - 9.0] kcal·mol^{-1} and [0.6 - 3.0] kcal·mol^{-1} for ACE, respectively. For such low barriers, of course, even small absolute variations imply large kinetic differences, and cannot be neglected, especially when the change of sign implies going from a barrierless reaction to one with a barrier. Fortunately, the best composite methods employed differ by less than 0.5 kcal·mol^{-1} for all the species considered. The DFT methods present discrepancies associated with both the method and the basis set employed, with the most glaring difference being observed in the CI+ETH reaction at the rev-DSDPBEP86-D3(BJ) level. Nonetheless, jun-ChS and SVECV-f12 values differ by only 0.04 kcal·mol^{-1}. This gives further support to our assertion that, with few exceptions, slightly different geometries (especially those of TSs) do not affect in a significant way the barrier heights computed by the best composite methods (however, this is not the case when B3LYP geometries are being used, like in CBS-QB3 or G4 for instance). In the other cases, including TSM which is the species we are mostly interested in, the values are larger.

Thus, the difference among methods, even if quantitatively significant, does not afford qualitative differences in the conclusions.

Table 4. Barrier (in kcal·mol^{-1}) and enthalpy of reaction (in kcal·mol^{-1}at 298 K) for the five dipolar molecules in reactions (1) and (2) with ETH and ACE.

		BARRIER (Δ(E + ZPE) of TS)									
		Ethylene					*Acetylene*				
Method	Basis Set	O$_3$	SO$_2$	CH$_2$OO	CH$_2$SO	CH$_2$SCH$_2$	O$_3$	SO$_2$	CH$_2$OO	CH$_2$SO	CH$_2$SCH$_2$
CBS-QB3		0.70	49.97	0.17	20.63	5.03	4.42	52.33	1.82	21.54	6.32
G4		4.58	50.96	1.20	21.78	7.10	8.99	54.02	2.98	22.85	8.37
W1BD		4.69	52.75	1.31	23.32	7.97	8.44	55.64	2.72	24.09	9.00
ωB97X-D	jun-cc-pV(T+d)Z	3.75	54.97	1.24	24.72	9.43	7.30	57.35	2.83	25.28	10.33
M06-2X-D3	jun-cc-pV(T+d)Z	2.50	50.93	0.12	22.56	7.63	5.75	54.10	1.69	23.54	8.49
rev-DSD	jun-cc-pV(T+d)Z	2.35	50.45	-0.88	26.28	4.90	7.47	54.15	0.65	21.44	6.28
CCSD(T)	cc-pV(T+d)Z[a]	3.6	51.0				8.0	54.7			
CCSD(T)-F12	pVDZ-F12						4.96	53.38			
	pVTZ-F12						5.32	54.47			
jun-ChS [b]	CBS	3.92	51.67	0.87	22.16	7.22	7.80	54.78	2.70	23.34	8.62
SVECV-f12 [c]	CBS	4.05	51.56	0.83	22.38	7.14	7.70	54.77	2.39	23.49	8.32
		ENDO/EXOTHERMICITY(ΔH of Products)									
		Ethylene					*Acetylene*				
Method	Basis Set	O$_3$	SO$_2$	CH$_2$OO	CH$_2$SO	CH$_2$SCH$_2$	O$_3$	SO$_2$	CH$_2$OO	CH$_2$SO	CH$_2$SCH$_2$
CBS-QB3		-55.75	16.48	-62.98	-27.72	-74.65	-62.27	7.23	-75.50	-42.97	-89.16
G4		-51.95	17.17	-61.02	-27.42	-73.03	-58.95	7.56	-73.89	-42.75	-87.42
W1BD		-54.59	17.36	-63.37	-27.68	-74.22	-61.82	7.46	-76.40	-43.20	-88.77
ωB97X-D	jun-cc-pV(T+d)Z	-58.65	15.71	-63.88	-29.48	-77.00	-67.29	4.02	-79.05	-47.04	-92.86
M06-2X-D3	jun-cc-pV(T+d)Z	-69.06	7.70	-67.20	-33.50	-76.42	-75.11	-1.49	-79.95	-48.76	-90.36
rev-DSD	jun-cc-pV(T+d)Z	-51.22	16.58	-65.28	-29.51	-76.42	-58.25	6.87	-78.27	-44.96	-90.58
jun-ChS [b]	CBS	-54.29	17.12	-61.98	-27.60	-73.91	-61.59	7.20	-74.85	-42.84	-88.04
SVECV-f12 [c]	CBS	-55.75	16.71	-63.18	-28.30	-75.24	-63.01	6.68	-76.17	-43.80	-89.66

[a] ref. [36] [b] using rev-DSDPBEP86-D3(BJ)/jun-cc-pV(T+d)Z optimum geometries; [c] using M06-2X-D3/jun-cc-pV(T+d)Z optimum geometries.

Focusing on the average of the two best results (jun-ChS and SVECV-f12), the barriers for the CI + (ETH, ACE) reactions (0.85 and 2.55 kcal·mol^{-1}, respectively) are lower than those for O$_3$ (3.99 and 7.75 kcal·mol^{-1}). Comparing these latter barriers with the very accurate values obtained by Wheeler et al.[33] (3.4 and 7.7 kcal·mol^{-1}, respectively), we observed an extremely good agreement for ACE and a reasonable one for ETH. Table 1 in their work contains some other theoretical values obtained in previous studies, which point out the difficulty in predicting those barriers, especially due to what they call a protracted convergence with respect to the inclusion of electron correlation. Later on, Saito et al.[34] calculated a larger value of 5.3 kcal·mol^{-1} at the

RCCSDT/CBS level, which is closer to the experimental result of 4.7 ± 0.2 kcal·mol^{-1}.[104] In turn, our best values (4.1 kcal·mol^{-1} at the SVECV-f12 and 3.9 at the jun-ChS levels of theory) agree also quite well with experiment, while the largest and more recent calculation we are aware of, at the CCSD(T)-F12/VTZ-F12//CCSD(T)/cc-pVTZ level,[105] gave a value of 4.5 kcal·mol^{-1} for the activation energy. In the case of the reaction of O_3 with ACE, Cramer et al.[106] determined a value of 9.28 kcal·mol^{-1} at the CCSD(T)/CBS limit. The most recent study by Trogolo et al.[107] obtained a best estimate of 7.65 kcal·mol^{-1}, which agrees nicely with our results (7.70 kcal·mol^{-1} at the SVECV-f12 and 7.80 at the jun-ChS levels of theory). From this analysis, it is clear that our composite protocols are able to represent very well the reaction of O_3 with double and triple bonds, irrespective of the multireference character of its ground state.

Concerning the reaction of CI with ETH, the barrier heights obtained by Vereecken et al.[40] at the CCSD(T)/aVQZ//M06-2X level (0.63 kcal·mol^{-1}) and by Sun et al.[48] employing the dual-level HL composite method[108] (1.1 kcal·mol^{-1}) are in agreement with our best results. In the case of ACE, Sun et al.[48] obtained a barrier of 3.9 kcal·mol^{-1}, while we obtained a barrier of 2.7 and 2.4 kcal·mol^{-1} at the SVECV-f12 and jun-ChS levels of theory, respectively. Although our barrier is again lower than that of Sun et al., in both cases the barrier for the addition to ACE is three times larger than that for the addition to ETH.

The agreement of SVECV-f12 and jun-ChS composite methods among themselves, with other high-level calculations and with experiment permits a safe analysis of the addition of TSM to ETH and ACE, for which previous results are not available. The computed barriers are 7.2 (for jun-ChS) and 8.5 (for SVECV-f12) kcal·mol^{-1}, and 8.6 (for jun-ChS) and 8.3 kcal·mol^{-1} (for SVECV-f12), respectively. Thus, the TSM addition to double and triple bonds is even more similar than that of O_3 and CI. For the addition to ETH, the barrier for TSM is almost twice larger than

that of O_3, but in the case of ACE, they are comparable. This means that addition of TSM to triple bonds should proceed with a velocity comparable to that of O_3 with the difference, of course, that the ozonides can further decompose (giving the CI and a carbonyl compound) while the hydrogenated thiophenes obtained as a result of the reaction with TSM are stable. In fact, among the five dipolar reactants studied, the reactions of TSM + (ETH, ACE) are the most exothermic ones, followed by those of CI.

The addition of FSO and, especially, SO_2 is highly unfavorable, with the barriers being several times larger than those of the other species. FSO exhibits barriers which are approximately half of those of SO_2, which is consistent with the larger density at the critical point of the forming C-C bond with respect to the C-O bond (see Fig. 5). The asymmetric addition of FSO is led by the forming C-C bond, followed by the C-O bond (although probably still in a concerted fashion).

4. CONCLUSIONS

Several theoretical methods were used to investigate the reactants, products and transition states of the reactions between five dipolar species and ethylene or acetylene. The reactants were chosen substituting the central oxygen atom by the valence isoelectronic sulfur atom, and one or both the terminal oxygen atoms by the isoelectronic CH_2 moiety. Our main interest was centered on the study of the trends in this series of concerted additions, with the purpose of determining whether the reactivity of thioformaldehyde *S*-methylide (TSM) is similar to that of the reactive O_3 and CI toward multiple bonds, or closer to the unreactive FSO and SO_2 species.

After assessing the ability of the theoretical methods used for reproducing geometry and thermochemical trends (including considerations about the multireference character of reactants), reaction barriers were examined in detail. The results showed that barriers were well reproduced

in those cases where comparison was possible with high-level theoretical results or experiment. Armed with that knowledge, we were able to determine that the cycloadditions of TSM to ETH and ACE were similar to those of O_3. While going from TSM to O_3 nearly doubles the activation barrier for the cycloaddition to ETH, the corresponding reactions with ACE are ruled by comparable barriers. As byproducts of this research, accurate values were produced for the unknown barriers ruling the addition of FSO to ETH and ACE, namely 22.3 ± 0.1 and 23.4 ± 0.1 kcal·mol^{-1} respectively.

In a more general perspective, it was shown that the composite methods developed in our laboratories, jun-ChS and SVECV-f12, are valuable and accurate tools for the study of atmospheric chemistry processes.

Supporting Information

Cartesian coordinates of optimized geometries for all species studied in this work.

REFERENCES

[1]   R. Huisgen, G. Mloston, E. Langhals, *J. Am. Chem. Soc.* **1986**, *108*, 6401.

[2] A. Padwa, W. H. Pearson, *The Chemistry of Heterocyclic Compounds, Volume 59: Synthetic Applications of 1,3-Dipolar Cycloaddition Chemistry Toward Heterocycles and Natural Products*, John Wiley & Sons, New York **2002**.

[3] R. Huisgen, *Angew. Chem.* **1963**, *75*, 742.

[4] R. Huisgen, *J. Org. Chem.* **1976**, *41*, 403.

[5] R. Huisgen, *1,3-Dipolar Cycloaddition Chemistry*, Vol. 1, A. Pawda, Wiley Interscience, **1984**, pp. 1–176.

[6] M. Breugst, H.-U. Reissig, *Angew. Chem. Int. Ed.* **2020**, *59*, 12293.

[7] R. A. Firestone, *J. Org. Chem.* **1968**, *33*, 2285.

[8] K. N. Houk, R. A. Firestone, L. L. Munchausen, P. H. Mueller, B. H. Arison, L. A. Garcia, *J. Am. Chem. Soc.* **1985**, *107*, 7227.

[9] K. N. Houk, J. González, Y. Li, *Acc. Chem. Res.* **1995**, *28*, 81.

[10] L. Xu, C. E. Doubleday, K. N. Houk, *Angew. Chem.* **2009**, *121*, 2784.

[11] J. P. Snyder, *J. Am. Chem. Soc.* **1974**, *96*, 5005.

[12] A. J. Arduengo, E. M. Burgess, *J. Am. Chem. Soc.*, **1976**, *98*, 5020.

[13] A. J. Arduengo, E. M. Burgess, *J. Am. Chem. Soc.* **1976**, *98*, 5021.

[14] J. Fabian, U. Eckart, A. B. Jr. Hess, *Wiss. Z. Techn. Universität Dresden*, **1995**, *44*, 99.

[15] J. Fabian, A. B. Jr. Hess, *J. Org. Chem.* **1997**, *62*, 1766.

[16] R. M. Kellogg, *Tetrahedron* **1976**, *32*, 2165.

[17] J. Buter, S. Wassenaar, R. M. Kellogg, *J. Org. Chem.* **1972**, *37*, 4045.

[18] E. B. Knott, *J. Chem. Soc.* **1955**, 916.

[19] J. Fabian, G. Mlostoń, *Polish J. Chem.* **1999**, *73*, 669.

[20] R. Sustmann, W. Sicking, R. Huisgen, *Chem. Eur. J.* **2003**, *9*, 2245.

[21] Z. Salta, J. Lupi, V. Barone, O. N. Ventura, *ACS Earth Space Chem.* **2020**, *4*, 403.

[22] Z. Salta, J. Lupi, N. Tasinato, V. Barone, O. N. Ventura, *Chem. Phys. Lett.* **2020**, *739*, 136963.

[23] Z. Salta, M. E. Segovia, A. Katz, N. Tasinato, V. Barone, O. N. Ventura, *J. Org. Chem.* **2021**, *86*, 2941.

[24] S. Jackson, L. A. Hull, *J. Org. Chem.* **1976**, *41*, 3340.

[25] K. Griesbaum, Y. Dong, *J. Prakt. Chem.* **1997**, *339*, 575.

[26] O. Horie, G. K. Moortgat, *Acc. Chem. Res.* **1998**, *31*, 387.

[27] S. G. van Ornum, R. M. Champeau, R. Pariza, *Chem. Rev.* **2006**, *106*, 2990.

[28] A. Maranzana, G. Serra, A. Giordana, G. Tonachini, G. Barco, M. Causà, *J. Phys. Chem. A* **2005**, *109*, 10929.

[29] K. Schank, *Helv. Chim. Acta* **2004**, *87*, 2074.

[30] S. P. Walch, W. A. III. Goddard, *J. Am. Chem. Soc.* **1975**, *97*, 5319.

[31] S. D. Kahn, W. J. Hehre, J. A. Pople, *J. Am. Chem. Soc.* **1987**, *109*, 1871.

[32] P. C. Hiberty, C. Leforestier, *J. Am. Chem. Soc.* **1978**, *100*, 2012.

[33] S. W. Wheeler, D. H. Ess, K. N. Houk, *J. Phys. Chem. A* **2008,** *112*, 1798.

[34] T. Saito, S. Nishihara, Y. Kataoka, Y. Nakanishi, Y. Kitagawa, T. Kawakami, S. Yamanaka, M. Okumura, K. Yamaguchi, *J. Phys. Chem. A* **2010,** *114*, 12116.

[35] G. H. Purser, *J. Chem. Educ.* **1999**, *76*, 1013.

[36] Y. Lan, S. E. Wheeler, K. N. Houk, *J. Chem. Theory Comput.* **2011**, *7*, 2104.

[37] T. Y. Takeshita, B. A. Lindquist, T. H. Jr. Dunning, *J. Phys. Chem. A* **2015**, *119*, 7683.

[38] T. H. Jr. Dunning, L. T. Xu, T. Y. Takeshita, B. A. Lindquist, *J. Phys. Chem. A* **2016**, *120*, 1763.

[39] B. Braïda, S. E. Galembeck, P. C. Hiberty, *J. Chem. Theory Comput.* **2017**, *13*, 3228.

[40] L. Vereecken, J. S. Francisco, *Chem. Soc. Rev.* **2012**, *41*, 6259.

[41] H. G. Kjaergaard, T. Kurtén, L. B. Nielsen, S. Jørgensen, P. O. Wennberg, *J. Phys. Chem. Lett.* **2013**, *4*, 2525.

[42] A. Jalan, J. W. Allen, W. H. Green, *Phys. Chem. Chem. Phys.* **2013**, *15*, 16841.

[43] W. Sander, *Angew. Chem., Int. Ed. Engl.* **1990**, *29*, 344.

[44] Y.-T. Su, Y.-H. Huang, H. A. Witek, Y.-P. Lee, *Science* **2013**, *340*, 174.

[45] M. Nakajima, Y. Endo, *J. Chem. Phys.* **2013**, *139*, 101103.

[46] L. Vereecken, H. Harder, A. Novelli, *Phys. Chem. Chem. Phys.* **2014**, *16*, 4039.

[47] Z. L. Buras, R. M. I. Elsamra, A. Jalan, J. E. Middaugh, W. H. Green, *J. Phys. Chem. A* **2014**, *118*, 1997.

[48] C. Sun, B. Xu, L. Lv, S. Zhang, *Phys. Chem. Chem. Phys.* **2019**, *21*, 16583.

[49] N. Pelloux-Leon, Y. Vallee, *Gas-Phase Reactions in Organic Synthesis*, Gordon and Breach, Amsterdam **1998**.

[50] B. Zwanenburg, *Recl. Trav. Chim. Pays-Bas* **1982**, *10*, 1.

[51] E. Block, R. E. Penn, R. J. Olson, P. F. Sherwin, *J. Am. Chem. Soc.* **1976**, *98*, 1264.

[52] E. Block, H. Bock, S. Mohmand, P. Rosmus, B. Solouki, *Angew. Chem.* **1976**, *88*, 380.

[53] E. Block, E. R. Corey, R. E. Penn, T. L. Renken, P. F. Sherwin, H. Bock, T. Hirabayashi, S. Mohmand, B. Solouki, *J. Am. Chem. Soc.* **1982**, *104*, 3119.

[54] O. N. Ventura, M. Kieninger, P. A. Denis, R. E. Cachau, *Chem. Phys. Lett.* **2002**, *355*, 207.

[55] R. Arnaud, P. Juvin, Y. Vallée, *J. Org. Chem.* **1999,** *64,* 8880.

[56] J.-D. Chai, Head-Gordon, *Phys. Chem. Chem. Phys*. **2008**, *10*, 6615.

[57] Y. Zhao, D. G. Truhlar, *Theor. Chem. Acc.* **2008**, *120*, 215.

[58] G. Santra, N. Sylvetsky, J. M. Martin, *J. Phys. Chem. A* **2019**, *123*, 5129.

[59] E. Papajak, J. Zheng, X. Xu, H. R. Leverentz, D. G. Truhlar, *J. Chem. Theory Comput.* **2011**, *7*, 3027.

[60] N. X. Wang, A. K. Wilson, *J. Phys. Chem. A* **2005**, *109*, 7187.

[61] V. Barone, G. Ceselin, M. Fusé, N. Tasinato, *Frontiers in Chemistry* **2020**, 8, 584203.

[62] S. Grimme, J. Antony, S. Ehrlich, H. Krieg, *J. Chem. Phys*. **2010**, *132*, 154104.

[63] E. Caldeweyher, C. Bannwarth, S. Grimme, *J. Chem. Phys.* **2017**, *147*, 034112.

[64] J. A. Jr. Montgomery, M. J. Frisch, J. W. Ochterski, G. A. Petersson, *J. Chem. Phys.* **1999**, *110*, 2822.

[65] L. A. Curtiss, P. C. Redfern, K. Raghavachari, *J. Chem. Phys.* **2007**, *126*, 084108.

[66] E. C. Barnes, G. A. Petersson, J. A. Jr. Montgomery, M. J. Frisch, J. Martin, *J. Chem. Theory Comput.* **2009**, *5*, 2687.

[67] O. N. Ventura, M. Kieninger, A. Katz, M. Vega-Teijido, M. E. Segovia, K. Irving, *Int. J. Quantum Chem.* **2021**, *121*, e26745.

[68] S. Alessandrini, V. Barone, C. Puzzarini, *J. Chem. Theory Comput.* **2020**, *16*, 988.

[69] V. Barone, J. Lupi, Z. Salta, N. Tasinato, *J. Chem. Theory Comput.* **2021**, *17*, 8, 4913.

[70] G. Knizia, T. B. Adler, H.-J. Werner, *J. Chem. Phys.* **2009**, *130*, 054104.

[71] T. Helgaker, W. Klopper, H. Koch, J. Noga, *J. Chem. Phys.* **1997**, *106*, 9639.

[72] D. Kreplin, P. J. Knowles, H.-J. Werner, *J. Chem. Phys.* **2019**, *150*, 194106.

[73] J. Finley, P- Å. Malmqvist, B. O. Roos, L. Serrano-Andrés, *Chem. Phys. Lett.* **1998**, *288*, 299.

[74] K. Fukui, *Acc. Chem. Res.* **1981**, *14*, 363.

[75] F. Weinhold, J. E. Carpenter, *The Structure of Small Molecules and Ions*, R. Naaman, Z. Vager Eds., Plenum **1988**.

[76] P. S. V. Kumar, V. Raghavendra, V. Subramanian, *J. Chem. Sci*. **2016**, *128*, 1527.

[77] Gaussian 16, Revision C.01, M. J. Frisch, G. W. Trucks, H. B. Schlegel, G. E. Scuseria, M. A. Robb, J. R. Cheeseman, G. Scalmani, V. Barone, G. A. Petersson, H. Nakatsuji, X. Li, M. Caricato, A. V. Marenich, J. Bloino, B. G. Janesko, R. Gomperts, B. Mennucci, H. P. Hratchian, J. V. Ortiz, A. F. Izmaylov, J. L. Sonnenberg, D. Williams-Young, F. Ding, F. Lipparini, F. Egidi, J. Goings, B. Peng, A. Petrone, T. Henderson, D. Ranasinghe, V. G. Zakrzewski, J. Gao, N. Rega, G. Zheng, W. Liang, M. Hada, M. Ehara, K. Toyota, R. Fukuda, J. Hasegawa, M. Ishida, T. Nakajima, Y. Honda, O. Kitao, H. Nakai, T. Vreven, K. Throssell, J. A. Montgomery, Jr., J. E. Peralta, F. Ogliaro, M. J. Bearpark, J. J. Heyd, E. N. Brothers, K. N. Kudin, V. N. Staroverov, T. A. Keith, R. Kobayashi, J. Normand, K. Raghavachari, A. P. Rendell, J. C. Burant, S. S. Iyengar, J. Tomasi, M. Cossi, J. M. Millam, M. Klene, C. Adamo, R. Cammi, J. W. Ochterski, R. L. Martin, K. Morokuma, O. Farkas, J. B. Foresman, and D. J. Fox, Gaussian, Inc., Wallingford CT, **2016**.

[78] MOLPRO, version 19.1, a package of ab initio programs, H.-J. Werner, P. J. Knowles, G. Knizia, F. R. Manby, M. Schütz, and others, see https://www.molpro.net. **2020**.

[79] AIM2000, *A Program to Analyze and Visualize Atoms in Molecules*, Version 2, https://www.chemistry.mcmaster.ca/aimpac/imagemap/imagemap.htm

[80] G. Ceselin, V. Barone, N. Tasinato, *J. Chem. Theory Comput*. **2021**, *17*, 7290.

[81] G. Herzberg, *Electronic spectra and electronic structure of polyatomic molecules*, Van Nostrand, New York **1966**.

[82] K. Kuchitsu, *Structure of Free Polyatomic Molecules - Basic Data*. Springer, Berlin **1998**.

[83] M. C. McCarthy, L. Cheng, K. N. Crabtree, O. Jr.Martinez, T. L. Nguyen, C. C. Womack, J. F. Stanton, *J. Phys. Chem. Lett.* 2013, *4*, 4133.

[84] J. Demaison, N. Vogt, D. N. Ksenafontov, *J. Mol. Struct*. **2020**, *1206*, 127976.

[85] T. J. Lee, J. E. Rice, G. E. Scuseria, H. F. Schaefer, *Theor. Chim. Acta* **1989**, *75*, 81.

[86] T. J. Lee, P. R. Taylor, *Int. J. Quantum Chem.: Quantum Chem. Symp. 23* **1989**, 199.

[87] T. J. Lee, G. E. Scuseria, *Quantum Mechanical Electronic Structure Calculations with Chemical Accuracy*, Kluwer Academic, Dordrecht **1995**.

[88] D. Jayatilaka, T. J. Lee, *J. Chem. Phys.* **1993**, *98*, 9734.

[89] M. L. Leininger, I. M. B. Nielsen, T. D. Crawford, C. L. Janssen, *Chem. Phys. Lett.* **2000**, *328*, 431.

[90] C. L. Janssen, I. M. B. Nielsen, *Chem. Phys. Lett.* **1998**, *290*, 423.

[91] T. J. Lee, *Chem. Phys. Lett.* **2003**, *372*, 362.

[92] S. R. Langhoff, C. W. Bauschlicher, *Annu. Rev. Phys. Chem.* **1988**, *39*, 181.

[93] J. Wang, S. Manivasagam, A. K. Wilson, *J. Chem. Theory Comput.* **2015**, *11*, 5865.

[94] L. Margules, M. E. Sanz, S. Kassi, D. Petitprez, G. Wlodarczak, J. C. Lopez, J. E. Boggs, *Chem. Phys.* **2001**, *263*, 19.

[95] J. R. During, Y. S. Li, D. T. During, *J. Chem. Phys.* **1981**, *74*, 1564.

[96] T. M. El-Gogary, *Spectrochim. Acta A* **2001**, *57*, 1405.

[97] A. D. Boese, R. Boese, *Cryst. Growth Des.* **2015**, *15*, 1073.

[98] J. Grant Hill, A. C. Legon, *Int. J. Quantum Chem.* **2019**, *119*, e25885.

[99] L. R. Domingo, M. T. Picher, *Tetrahedron* **2004**, *60*, 5053.

[100] S. J. Grabowski, *Molecules* **2015**, *20*, 11297.

[101] S. Berski, Z. Latajka, *Int. J. Quantum Chem.* **2011**, *111*, 2378.

[102] J. Friis, G. K. H. Madsen, F. K Larsen, B. Jiang, K. Marthinsen, R. Holmstad, *J. Chem. Phys.* **2003**, *119*, 11359.

[103] L. A. Terrabuio, T. Q. Teodoro, M. G. Rachid, R. L. Haiduke, *J. Phys. Chem. A* **2013**, *117*, 10489.

[104] W. B. DeMore, *Int. J. Chem. Kinet.* **1969**, *1*, 209.

[105] O. B. Gadzhiev, S. K. Ignatov, B. E. Krisyuk, A. V. Maiorov, S. Gangopadhyay, A. E. Masunov, *J. Phys. Chem. A* **2012**, *116*, 10420.

[106] D. Cremer, E. Kraka, R. Crehuet, J. Anglada, J. Grafenstein, *Chem. Phys. Lett.* **2001**, *347*, 268.

[107] D. Trogolo, J. S. Arey, P. R. Tentscher, *J. Phys. Chem. A* **2019**, *123*, 517.

[108] J. A. Miller, S. J. Klippenstein, *J. Phys. Chem. A* **2003**, *107*, 2680.